Traction Forces Generated by Locomoting Keratocytes

Juliet Lee,* Michelle Leonard,* Tim Oliver,* Akira Ishihara,* and Ken Jacobson*‡

*Department of Cell Biology and Anatomy and ‡Lineberger Comprehensive Cancer Center, University of North Carolina at Chapel Hill, Chapel Hill, North Carolina 27599-7090

Abstract. Traction forces produced by moving fibroblasts have been observed as distortions in flexible substrata including wrinkling of thin, silicone rubber films. Traction forces generated by fibroblast lamellae were thought to represent the forces required to move the cell forwards. However, traction forces could not be detected with faster moving cell types such as leukocytes and growth cones (Harris, A. K., D. Stopak, and P. Wild. 1981. *Nature (Lond.)*. 290:249–251). We have developed a new assay in which traction forces produced by rapidly locomoting fish keratocytes can be detected by the two-dimensional displacements of small beads embedded in the plane of an elastic substratum. Traction forces were not detected at the rapidly extending front edge of the cell. Instead the largest traction forces were exerted perpendicular to the left and right cell margins. The maximum traction forces exerted by keratocytes were estimated to be $\sim 2 \times 10^{-8}$ N. The pattern of traction forces can be related to the locomotion of a single keratocyte in terms of lamellar contractility and area of close cell–substratum contact.

To move cells must exert traction forces upon the substratum. This involves the temporal and spatial regulation of numerous force generating molecular motors. Yet an understanding of how and where moving cells generate traction forces, represents a major gap in our knowledge of cell locomotion. This paper presents the first measurements of the traction forces generated by rapidly moving cells.

Traction forces produced by moving fibroblasts were first observed as distortions in flexible substrata that caused wrinkling of thin, silicone rubber films (Harris et al., 1980). These traction forces act inwards, relative to the extending lamella and retracting edge, leading to compression of the substratum such that wrinkles are formed perpendicular to the direction of lamellar extension. Wrinkles were thought to be formed by an actomyosin-based contraction of the cytoskeleton which is transmitted to the substratum via focal adhesions located just behind the extending edge and trailing cell edge. Traction forces generated by fibroblast lamellae were thought to represent the forces required to move the cell forwards along the substratum. It was therefore surprising to find that traction forces generated by faster moving cell types such as leukocytes and growth cones could not be detected (Harris, 1981), since it was assumed that larger traction forces would be required for faster locomotion. However, slow moving cells such as fibroblasts form strong focal adhesions to the substratum whereas faster moving cells tend to form weaker close contacts (Couchman and Reese, 1979). In addition large numbers of actin stress fibers are found in slower moving cells, implying greater cytoskeletal contractility. Therefore rapid cell locomotion appears to rely on both weaker cell substratum adhesions and cytoskeletal contractility.

To learn more about the traction forces required for rapid locomotion, we have modified the traction force assay of Harris to detect the size and orientation of traction forces generated by fish epithelial keratocytes, without wrinkling the substratum. Instead these forces can be detected as two-dimensional displacements of marker beads embedded in the substratum. Such displacements are easier to quantitate than wrinkles and so provide more accurate information about the location and orientation of traction forces. In addition the use of a simple-shaped cell type such as the fish keratocyte allows the distribution of the traction forces to be related to the movement of the entire cell. The fact that keratocyte cell shape is maintained during locomotion means that the steady-state distribution of traction forces may be observed.

Materials and Methods

Silicone Substrata

A Rappaport chamber was used consisting of a thick walled Pyrex cylinder (22 × 8 mm) to which a circular glass coverslip has been sealed to its base with vacuum grease (see Fig. 1 *a*). Silicone fluid (dimethylpolysiloxane, viscosity = 12,500 centipoise; Sigma Chemical Co., St. Louis, MO) was poured into the base of the chamber and allowed to spread evenly. Latex beads (1-μm diam) were sprinkled over the surface with a fine brush. Cross-linking of the top layer of silicone oil was achieved by placing the chamber into a modified glow discharge apparatus (Polaron sputter coater E5100)

Address all correspondence to K. Jacobson, Department of Cell Biology and Anatomy, 108 Taylor Hall, Chapel Hill, Chapel Hill, NC 27599-7090. Ph: (919) 966-5703. Fax: (919) 966-1856.

M. Leonard's present address is Innovision Corp., Durham, NC 27113.

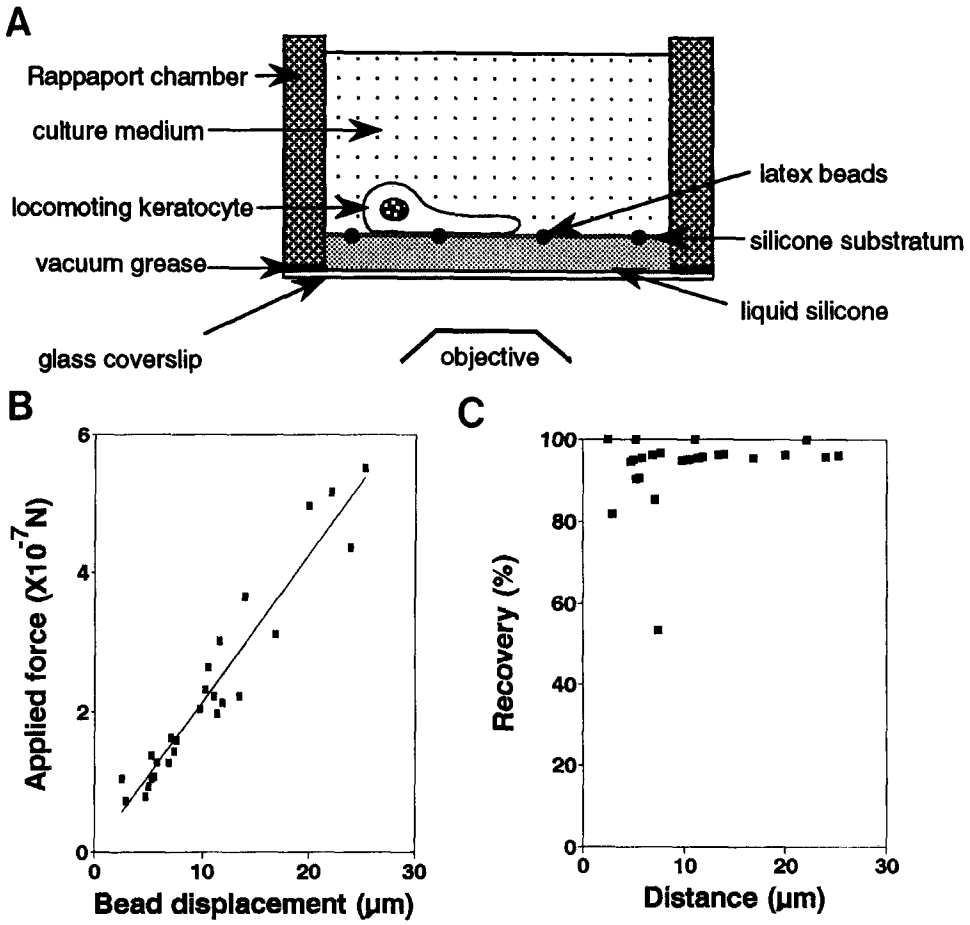

Figure 1. (*A*) A schematic diagram of modified traction force assay. The Rappaport chamber consists of a thick-walled Pyrex cylinder to which a circular glass coverslip has been sealed to its base with vacuum grease. Inside, resting on silicone fluid, is a thin film of crosslinked silicone into which small latex beads have been embedded. (*B*) Applied forces required for various bead displacements on an elastic substratum. (*C*) Percent recovery of the bead towards its original undisplaced position after it is released from the microneedle.

at an air pressure of 0.15 Torr and a target height of 60 mm. Voltage was applied to maintain a constant current of ~2 mA for 2 s. Weaker "hyper-compliant" substrata were produced by reducing the time in the glow discharge.

Calibration of Substratum

Force calibration needles that were highly flexible with sharply pointed tips were made using a programmable pipette puller (P87 Brown Flaming). Stiffer reference needles were pulled by hand and calibrated by plotting the amount of tip deflection produced by single weights in the range of 0.35–6.1 mg made from varying lengths of copper wire. The force required to displace a bead in a silicone substratum was measured by reproducing the deflection of the tip of the highly flexible microneedle with the stiffer calibrated reference microneedle. Tip deflection in both needles was proportional to the force applied. Video images of the calibration experiments were recorded and used to obtain tip deflection for a given bead displacement. This was repeated about 20 times with beads randomly selected throughout the substratum. The compliance of a substratum was given by the slope of the displacement versus force plot (see Fig. 1 *B*). The percent recovery of a bead toward its original undisplaced position was measured 15 s after the bead was released from the microneedle. Percent recovery = $(p - q)/p \times 100$, where p = original bead displacement and q = bead displacement after recovery.

Cell Culture

Keratocytes from hybrid populations of the Molly fish Poecillia sphenops were cultured as described previously for goldfish Carassius auratus (Lee et al., 1993*a*). They were then disaggregated by adding Ca^{2+}-free PBS and trypsin in a 1:1 mixture and resuspended in a small (~50 μl) volume of culture medium which was then added to the Rappaport chambers that had been prefilled with medium.

Video Microscopy and Analysis of Bead Displacements

Observations of keratocytes were made at room temperature within glass Rappaport chambers (see Fig. 1 *A*) using differential interference microscopy. Interference reflection microscopy was performed according to Bereiter-Hahn et al. (1981). The video microscope system was composed of a Zeiss inverted microscope (Axiovert 10), a 20×/0.5 NA plan neofluor

Figure 2. (*A–C*) Computer images of selected bead displacements (numbered *1–5*) induced by keratocyte locomotion on an elastic substratum. The path of the cell's centroid (*c*) is shown consisting of three sections (*red*, *green* and *blue*) with each color representing ~40 s of cell locomotion that match corresponding time intervals for bead displacements with respect to the substratum. (*A*) Bead displacements (*red*) are negligible as the cell approaches. (*B*) Maximum bead (*1, 2, 4,* and *5*) displacements (*green*) occur inwards, perpendicular to the lateral cell margins, at the rear, below the equator of the cell (*dotted line*). (*C*) The beads return toward their original positions (*blue*). (*D–F*) Bead displacements induced by the locomotion of a keratocyte on a hyper-compliant substratum. Colored sections correspond to consecutive, 26-s time intervals. (*D*) Beads *2* and *3* are displaced forwards (*red*). Beads *1* and *4* are displaced inwards, perpendicular to lateral cell margins. (*E*) Forward displacement (*green*) of beads *2* and *3* continues beneath the extending lamella, and to a lesser extent for bead *1*. Bead *4* is displaced inwards, perpendicular to the rear, lateral cell margin. (*F*) Beads *1–3* make their largest inward displacements (*blue*) beneath the cell rear. Bead *4* continues to be displaced in the direction of cell locomotion. Bar, 10 μm.

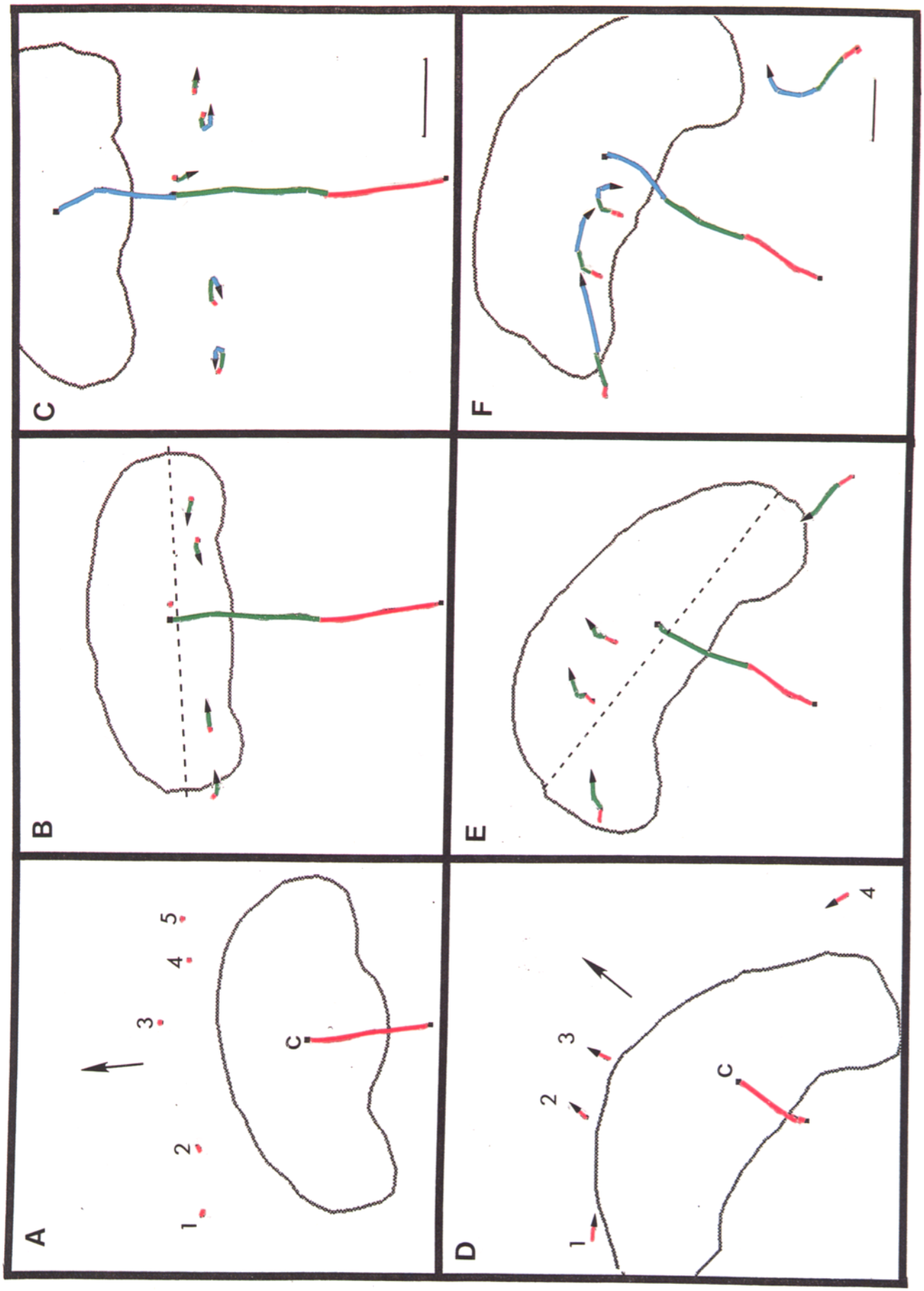

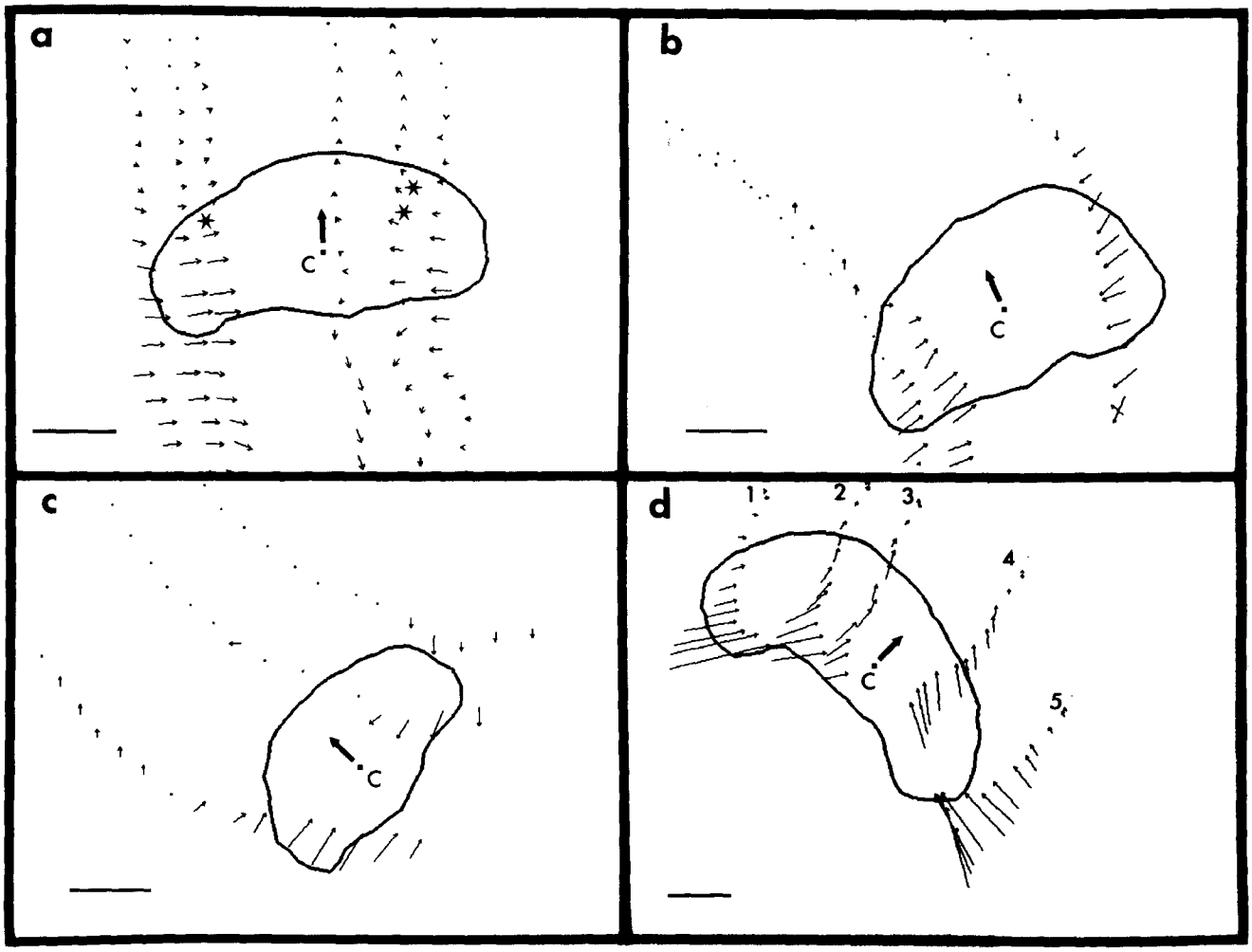

Figure 3. (*a*) A vector map of traction forces exerted on an elastic substratum (compliance = 8×10^{-9} N/μm) with respect to the centroid (*C*) of the cell in Figure 2 *a*. The change in magnitude and direction of traction forces (indicated by length and direction of *arrows*, respectively) exerted at a given bead location, with increasing time, can be seen by reading downward, opposite to the direction of locomotion (*arrow*). The largest traction forces are directed inwards, perpendicular to the lateral cell margins. They are not detected at the front of the extending lamella. Small traction forces are oriented inwards, perpendicular to the lateral edges of the extending lamella (*asterisks*). (*b* and *c*) Vector maps of traction forces exerted on elastic substrata. The compliances of the substrata were 1.06×10^{-8} and 2.14×10^{-8} N/μm, respectively. Because of smaller displacements the vectors shown in the figures *b* and *c* were amplified fivefold. (*d*) Bead displacement vectors occurring on a hyper-compliant substratum, with respect to the centroid (*C*) of the cell in Figure 2 *d*. They increase in size towards the rear of the cell and are oriented inwards, perpendicular to the cell edge. Displacement vectors (e.g., bead *3*) that exist beneath the extending lamella tend to be oriented in the direction of cell motion. This is thought to result indirectly from lateral compression of the substratum by the moving keratocyte. Bar, 10 μm.

objective, a 0.55 NA long-distance condenser, and a Hamamatsu C2400 video camera with a 4× adapter. Images of moving keratocytes (16 frames averaged) were acquired every 5 s and recorded on an optical memory disc recorder (Panasonic TQ-2028F) during about 10 min of locomotion. Image-1 software (Universal Imaging, West Chester, PA) was used to acquire, record, and process images.

Vector diagrams were produced by calculating the displaced and undisturbed bead positions with respect to the moving cell's centroid at every time interval (see Fig. 3, *a* and *b*, 20 s; *c*, 50 s; and *d*, 10 s). These relative bead positions were replotted in reference to a given cell centroid position (*C*). Lines drawn from the each bead's undisturbed position to its displaced position gave the size and direction of bead displacement with respect to the cell's stationary frame of reference at *C*. The cell centroid positions were obtained by manually fitting ellipsoids onto the keratocyte cell margin. Although keratocytes generally maintain an almost constant shape during locomotion, some small changes in shape do occur. To estimate errors from such shape changes, cell centroid positions were obtained in three independent measurements. The maximum uncertainty was ± 1.84 μm either side of the original trajectory. Vector diagrams drawn from the three different centroid measurements did not vary significantly.

Results

Elastic substrata were made by using a glow discharge device to cross-link a thin film of silicone oil within a glass Rappaport chamber (Fig. 1 *A*). This technique allows the reproducible manufacture of elastic substrata with similar compliances. In addition substrata with a range of compliances can be made by varying the degree of crosslinking. Compliances were measured with a calibrated glass microneedle (Harris et al., 1980; Yoneda, 1960) and were found to be similar within a given substratum. Substrata with compliances of ei-

Table I. Estimation of Maximum Traction Forces

Experiment number	Substratum type	Compliance	Bead #	Maximal displacement	Force
		($\times 10^{-8}$ N/μm)		(μm)	($\times 10^{-8}$ N)
1	Elastic	1.06	1	0.914	0.97
			2	0.750	0.79
			3	1.172	1.24
2	Elastic	1.06	1	0.990	1.05
			2	1.260	1.33
3	Elastic	2.14	1	1.104	2.36
			2	0.762	1.63
4	Elastic	1.26	1	1.459	1.84
5	Hyper-complaint	0.46	1	3.850	1.77
			2	4.430	2.03
			3	2.880	1.32
6	Elastic	0.80*	1	2.930	2.34
			2	2.967	2.37
			3	2.930	2.34

In each experiment two or three beads which displayed the largest displacements were selected and their maximal displacements obtained. The traction force exerted on each bead was calculated by multiplying the substratum compliance and the maximal displacement.
* The compliance of this substratum was not measured but estimated according to its relative elasticity.

ther $\sim 2 \times 10^{-8}$ or $\sim 5 \times 10^{-9}$ N/μm were preselected prior to plating keratocytes. These substrata are referred as "elastic" and "hyper-compliant" substrata, respectively. On the elastic substrata, bead displacements were proportional to the force applied to them (Fig. 1 *B*). In addition nearly all beads recovered to their original positions (Fig. 1 *C*). The half time for recovery was ~0.5 s indicating a small amount of viscous drag. On the hyper-compliant substrata, while bead displacements were proportional to the applied force, the beads recovered only 30–60% towards their original position (data not shown). In addition the half-time for recovery was ~3 s. These observations indicate that hypercompliant substrata exhibit both plastic and viscoelastic behavior.

Locomoting keratocytes produced a symmetrical, steady-state pattern of bead displacements on both elastic (Fig. 2, *A–C*) and hyper-compliant substrata (Fig. 2, *D–F*) without any apparent effect on cell morphology or speed. Use of hypercompliant substrata was essential in determining whether our modified traction force assay was working since bead displacements are large and easily visible during play back of video sequences. In addition they allowed the detection of traction forces generated by greater numbers of cells since even the "weakest" of cells could produce marked bead displacements. During locomotion, beads close to the lateral cell margins were displaced inwards, perpendicular to the cell edge (Fig. 2, *B* and *E*). The largest bead displacements were found for beads within the rear half of the cell (Fig. 2, *B* and *F*). Inward, lateral displacements were smaller for beads that were closer to the center of the cell (Fig. 2 *B*, bead *3*; Fig. 2 *F*, beads *2* and *3*). Following maximum displacement, beads within elastic substrata relaxed towards their undisplaced positions, when the rear cell margin passed over them (Fig. 2 *C*). The degree of recovery was generally decreased compared with that of micromanipulated beads. This discrepancy is thought to be due to the differences in applying a field of forces, in the former case, compared to the application of a highly localized, point force from a microneedle. Bead displacements within hyper-compliant substrata were much larger than within elastic ones. In addition beads were displaced forwards in front of the cell to a maximum, as it approached (Fig. 2 *D*, beads *2* and *3*). This maximum displacement is maintained as the leading edge passes over the bead and was followed by a less than 50% recovery of beads to their original positions (data not shown); this incomplete recovery was consistent with the plastic and viscous properties of hyper-compliant substrata.

Vector diagrams (Fig. 3) show the relative sizes and directions of bead displacements with respect to the cell. For elastic substrata (Fig. 3, *a*–c) bead displacements were proportional to the traction force applied (Fig. 1 *b*). Thus vectors represent the magnitude and direction of the traction forces generated by a locomoting keratocyte. Traction forces were generally not detectable at the front of the lamella. However, small traction forces ($\sim 7.5 \times 10^{-9}$ N) could be detected, oriented inwards with respect to the lateral edges of the extending lamella (Fig. 3 *A*). The largest traction forces were generated predominately within the rear half of the lamella (Fig. 3, *a–c*). They were oriented inwards, perpendicular to the lateral cell margins. Traction forces reached a maximum ($\sim 2 \times 10^{-8}$ N) at equatorial regions of the cell and were maintained within retracting regions at the rear. The maximum displacements of beads were measured for several cells (Table I). The calculated traction forces range from 1×10^{-8} to 2×10^{-8} N.

Bead displacement vectors within hyper-compliant substrata (Fig. 3 *d*) are not assumed to be proportional to applied traction forces. This is because the effects of their viscous and plastic properties cannot be separated from the elastic behaviour of these substrata. However, this vector map (Fig. 3 *d*) is qualitatively similar to those in Fig. 3 (*a–c*). In addition these substrata were about four times more sensitive to traction forces exerted on them than the elastic substrata. Thus smaller traction forces (detected as bead displacement vectors) could be observed that would otherwise not be visible within elastic substrata. Of all the cells observed (~20) no rearward oriented vectors were found at the

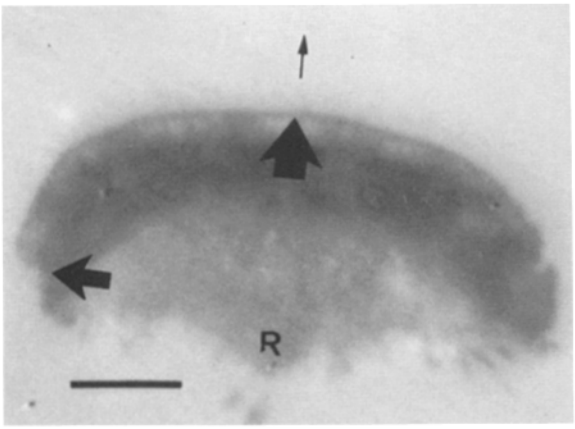

Figure 4. An interference reflection image of a keratocyte moving in the direction indicated (*small black arrow*). A broad region of close cell–substratum contact (*dark gray*) exists along the cell margin between the ventral cell surface and the substratum. This region is broadest adjacent to the most rapidly extending regions of the lamella (*large black arrowhead*) and narrowest close to retracting regions (*medium black arrowhead*). At the rear cell edge, where retraction is most rapid, no close contact exists (*R*), although the cell is in more distant contact with the substratum (*light gray region*). Bar, 10 μm.

front edge of the cell. Instead they tend to be oriented in the direction of cell motion (Fig. 3 *d*, beads *2–4*). The size of forward oriented vectors is significant. Therefore, we cannot exclude the possibility that these vectors obscure the detection of smaller rearward directed traction forces. Forward vectors are probably due to the secondary result of the strong inward traction forces generated at the lateral edges of the keratocyte. This is suggested by experiments on similar substrata where the lateral inward traction forces are simulated by compressing the substratum between microneedles (Oliver, T., manuscript in preparation). The largest displacements are found at the rear of the cell (Fig. 3 *d*, beads *1* and *5*) oriented inward and perpendicular to the cell margin in agreement with the other traction force vector maps (Fig. 3, *a–c*). These are largest closest to the cell edge and become progressively smaller toward the cell center (Fig. 3 *d*, compare beads *1–3*).

An interference reflection image of a moving keratocyte (Fig. 4) showed a region of close cell–substratum contact along the ventral cell margin. The broadest region was located adjacent to the most rapidly extending regions of the lamella and narrowest close to retracting regions. This pattern of close contacts has recently been confirmed using total internal reflection microscopy (Lee, J., and K. Jacobson, manuscript in preparation). Knowledge of the location of closest cell–substratum contacts is important in considering the sites of traction force generation. At the rear cell edge, where retraction was most rapid, no close contact existed, although the cell was in intermediate contact with the substratum.

Discussion

Our traction force assay allows the detection of traction forces generated by rapidly moving cells that are an order of magnitude less than those generated by fibroblasts. The traction forces exerted by keratocytes are estimated as $\sim 2 \times 10^{-8}$ N, while those exerted by fibroblasts are estimated as $\sim 2 \times 10^{-7}$ N (Harris, A., personal communication). The method not only detects weaker forces but also estimates the direction and the location of forces.

Traction Forces Are Not Detected at the Front of the Cell

One striking feature of our results is that traction forces were not detected in the front of extending keratocyte lamellae. This is in contrast to what was found for fibroblasts (Harris et al., 1980, 1981) where rearward oriented traction forces at the front of the cell were suggested to be directly involved in "propelling" the cell forward. Instead our data suggest that traction forces at the front of the cell are not required for cell movement. This raises the question of how the extension of the keratocyte lamella can occur without the production of traction forces. Firstly, a simple fluid dynamics calculation shows that a moving cell need exert only a very small force against the surrounding medium. Ignoring adhesion to the substratum, the only force required for forward cell motion is that needed to overcome the viscous drag of the medium. Assuming that a moving keratocyte is a disk, then the drag force will be $F = 32\eta\, r\, v/3$ (Berg, 1982) where η is the medium viscosity, r is the radius of the disk, and v is the velocity of the cell. In our case where $\eta \approx 1$ cP, $r \approx 30$ μm, $V \approx 1$ μm/s. This force is $\sim 3 \times 10^{-13}$ N and would not be detectable by our assay. Secondly, traction forces may be required to overcome frictional forces between the cell and substratum for the ventral cell surface to move along a surface. However, the actin meshwork is stationary with respect to the substratum at the front of the keratocyte (Theriot and Mitchison, 1991) indicating that there is no sliding of the ventral cell surface over the substratum.

How Traction Forces Are Involved in Keratocyte Locomotion

The fact that no rearward traction forces are detected at the front of the cell, is consistent with the hypothesis that lamellar extension occurs in a manner analogous to "growth" (Fig. 5 *A*; Evans, 1993). According to this idea, polymerization of actin filaments would have to occur predominately at the front edge of the cell, as has been shown in keratocytes (Theriot and Mitchison, 1991). For continued extension, the front edge must adhere to the substratum (Izzard and Lochner, 1980). In keratocytes a broad region of close cell substratum contact is found at the leading edge (Fig. 4). In addition, it appears that the contractility of the actin cytoskeleton at the front of the cell is low. This is indicated by the absence of inward directed traction forces in this region (Fig. 3) and by the behavior of photoactivated actin (Theriot and Mitchison, 1991). Low contractility at the front of the cell is consistent with the finding that lamellar extension and contraction of the cytoskeleton can occur as two separate events (Evans et al., 1993). In other words, extension can occur independently of contraction. As mentioned previously, the actin cytoskeleton is stationary with respect to the substratum at the front of the cell. However, if significant contractile forces are present then the cytoskeleton would "slip" rearwards with respect to the substratum (and leading edge) as was found in fibroblasts (Theriot and Mitchison, 1992). Thus low con-

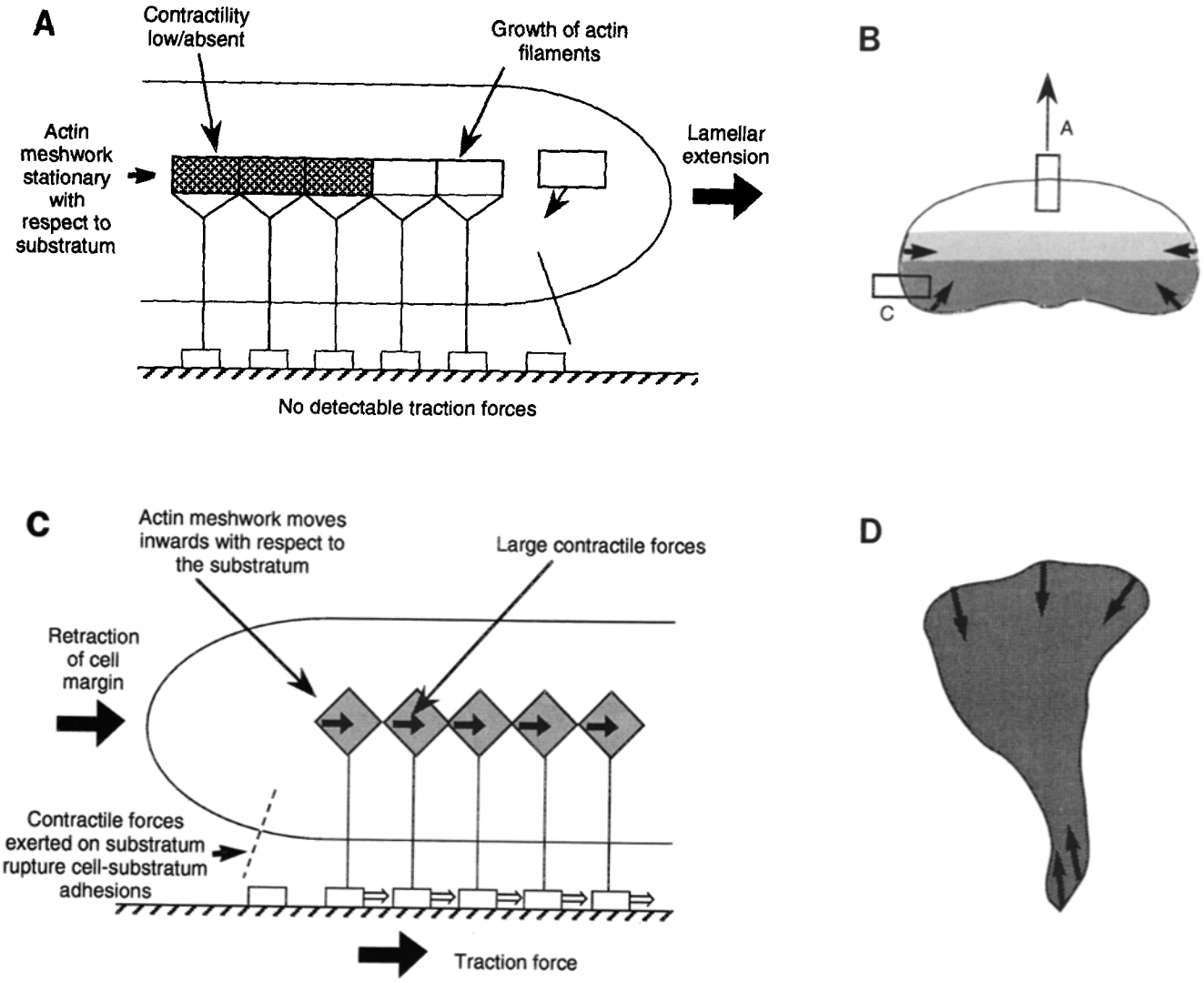

Figure 5. Diagram illustrating how traction force generation is related to the movement of a whole cell. (*A*) Lamellar extension in keratocytes (see *inset A* in *B*) may occur in a process analogous to "growth" which involves net polymerisation of actin filaments at the leading edge simultaneous with the formation of new cell–substratum adhesions. (*B*) Lamellar extension can occur without a contractile cytoskeleton (*white region*) and the production of detectable traction forces. At equatorial regions contractility of the cytoskeleton (*light grey region*) is great enough to deform the substratum without rupturing cell-substratum adhesions. (*C*) When the contractility of the cytoskeleton at the lateral edges of keratocytes (*inset C* in *b*) is great enough to deform the substratum and to rupture cell adhesions, the cell margin will retract. The rate of retraction will increase towards the rear of the cell as contractility increases and area of close cell–substratum adhesion decreases (compare with Fig. 4). However, cytoskeletal contractility can still exert traction on the substratum via remaining adhesions. (*D*) In the fibroblast traction forces are oriented inwards with respect to both front and rear edges (*bold arrows*) and contractility of the cytoskeleton is high throughout the cell.

tractility and relatively high cell–substratum adhesion favor lamellar extension (Fig. 5 *B, white region).*

The generation of traction forces is dependent both on the contractile strength of the cytoskeleton and cell–substratum adhesion. The requirement for a contractile cytoskeleton is indicated by finding that photoactivated actin marks move inwards with respect to the substratum (and cell edge) at the lateral edges of the keratocyte, corresponding to where the largest traction forces are seen (Lee, J., and J. A. Theriot, unpublished data). Increasing contractility of the cytoskeleton, toward the rear of the keratocyte is shown by the progressive, inward curvature of photoactivated actin marks at the rear of the cell (Lee et al., 1993*a*). Not only must contractility be great enough to deform the substratum but sufficient adhesions must exist to transmit contractile forces to the substratum. Thus although a large region of close contact exists at the front of the cell no traction forces are detected because contractility of the cytoskeleton is too low. The relative magnitude and position of inward oriented traction forces depends on the varying ratio of cytoskeletal contractility and adhesion strength (assuming area of close contact is proportional to adhesion strength at the cell margin) at different locations along the cell margin.

The largest traction forces are found at the equatorial region of the cell (Fig. 5 *B, light grey* region). The position of these forces coincides with a region of high cytoskeletal con-

tractility but which is counterbalanced by close cell-substratum contacts on either side of the cell. This leads to the development of tension perpendicular to the direction of cell motion as shown by parallel arrays of actin stress fibers that span the width of the cell (Bereiter-Hahn et al., 1981; Euteneur and Schliwa, 1984; Heath and Holifield, 1991). Increased tension within the cytoskeleton inhibits lamellar extension (Kolega, 1986; Lee et al., 1993*b*) such that the lateral cell margins neither extend nor retract in accord with the Graded Radial Extension model of keratocyte locomotion (Lee et al., 1993*a*).

At the rear of the keratocyte the contractility of the cytoskeleton is greatest (Fig. 5 *B*), but cell-substratum adhesion becomes weaker as indicated by the decreasing area of close contact towards the rear edge (Fig. 4). Increasing contractility together with decreasing adhesion strength leads to progressively increased rates of lamellar retraction towards the rear of the cell (Lee et al., 1993*a*). Thus, the traction forces generated by keratocytes provide the necessary mechanical force to overcome adhesion forces between cell and substratum (Fig. 5 *C*).

It is interesting to note that the traction forces produced by keratocytes are similar in magnitude to the contractile forces measured in retracting neurites and phagocytosing leukocytes (Heidemann, et al., 1990; Evans, et al., 1993). This suggests that actomyosin based contractility can generate forces of similar magnitudes in diverse motile phenomena (Oliver et al., 1994).

The Pattern of Traction Forces Is Related to the Mode of Cell Locomotion

In keratocytes broad close cell-substratum contacts and negligible lamellar contractility at the front of the cell favor rapid lamellar extension. Conversely, high contractility and an absence of close cell-substratum adhesions at the rear favor rapid retraction of the cell margin (Fig. 5 *B*). This marked asymmetry between front and rear of the keratocyte appears to be essential for the rapid, forward locomotion of these cells. Such asymmetry is much less apparent in fibroblasts (Fig. 5 *D*) where strong cell-substratum adhesions and high lamellar contractility (1×10^{-7} N as inferred from wrinkling silicone substrata; Harris, A., personal communication) exist at front and rear cell edges. Increased tension in the actin meshwork between front and rear of the cell may thus impede forward locomotion of fibroblasts. This is consistent with the observation that forward movement is slow and occurs in two discrete phases. Thus lamella extension proceeds until inhibited by increasing tension between front and rear of the cell. Following a short lag, retraction of the cell rear occurs and tension is released, leading to another phase of lamellar extension (Chen, 1979).

Although traction forces are generated by the same processes in keratocytes and fibroblasts, the spatial arrangement of cell-substratum adhesions and degree of lamellar contractility are the key determinants of the differences in pattern of traction forces generated by these two cell types and in their modes of locomotion.

The development of an assay to detect the traction forces generated by moving keratocytes provides an important new tool with which to study cell locomotion. In addition, traction forces detected by this assay are amenable to quantitative analyses, that can produce a more detailed map of the traction forces generated beneath a moving cell (Oliver, T., M. Dembo, A. Ishihara, and K. Jacobson, manuscript in preparation). The ability of manufacture substrata of various compliances means that this assay may be used to detect traction forces over a range of magnitudes and in various cell types.

We are especially grateful for the inspiration and advice provided by A. Harris, including his suggestion to use a glow discharge apparatus to cross-link silicone substrata. We thank B. Nicklas for his help with microneedle calibration; M. Dembo, E. Evans, and M. Peterson for their comments on this work together with D. Bray and A. Harris for their critical reading of this manuscript.

This work was supported by the National Institutes of Health.

Received for publication 18 May 1994 and in revised form 8 September 1994.

References

Bereiter-Hahn, J., R. Strohmeier, I. Kunzenbacher, K. Beck, and M. Voth. 1981. Locomotion of *Xenopus* epidermis cells in primary culture. *J. Cell Sci.* 52:289–311.

Berg, H. C. 1982. Random walks in biology. Princeton University Press, Princeton, NJ. 48–64.

Chen, W.-T. 1979. Induction of spreading during fibroblast movement. *J. Cell Biol.* 81:684–691.

Couchman, J. R., and D. A. Rees. 1979. The behavior of fibroblasts migrating from chick heart explants: changes in adhesion, locomotion and growth, and in the distribution of actomyosin and fibronectin. *J. Cell Sci.* 39:149–165.

Euteneur, U., and M. Schliwa. 1984. Persistent, directional motility of cells and cytoplasmic fragments in the absence of microtubules. *Nature (Lond.).* 319:58–61.

Evans, E. 1993. New physical concepts for cell amoeboid motion. *Biophys. J.* 64:1306–1322.

Evans, E., A. Leung, and D. Zhelev. 1993. Synchrony of cell spreading and contraction force as phagocytes engulf large pathogens. *J. Cell Biol.* 122:1295–1300.

Harris, A. K., P. Wild, and D. Stopak. 1980. Silicone rubber substrata: a new wrinkle in the study of cell locomotion. *Science (Wash. DC).* 208:177–179.

Harris, A. K., D. Stopak, and P. Wild. 1981. Fibroblast traction as a mechanism for collagen morphogenesis. *Nature (Lond.).* 290:249–251.

Heath, J. P., and B. F. Holifield. 1991. Cell locomotion. Actin alone in lamellipodia. *Nature (Lond.).* 352:107–108.

Heidemann, S. R., P. Lamoureux, and R. Buxbaum. 1990. Growth cone behavior and production of traction force. *J. Cell Biol.* 111:1949–1957.

Izzard, C. S., and L. R. Lochner. 1980. Formation of cell-to-substrate contacts during fibroblast motility: an interference reflexion study. *J. Cell Sci.* 42:81–116.

Kolega, J. 1986. Effects of mechanical tension on protrusive activity and microfilament and intermediate filament organization in an epidermal epithelium moving in culture. *J. Cell Biol.* 102:1400–1411.

Lee, J., A. Ishihara, J. A. Theriot, and K. Jacobson. 1993*a*. Principles of locomotion for simple-shaped cells. *Nature (Lond.).* 362:167–171.

Lee, J., A. Ishihara, and K. Jacobson. 1993*b*. *In* Cell Behaviour: Adhesion and Motility. The Society for Experimental Biology Symposium. Vol. 47. G. Jones, C. Wigley, and R. Warn, editors. The Company of Biologists Limited, London, UK. 73–89.

Oliver, T., J. Lee, and K. Jacobson. 1994. Forces exerted by locomoting cells. *Semin. Cell Biol.* 5:139–147.

Theriot, J. A., and T. J. Mitchison. 1991. Actin microfilament dynamics in locomoting cells. *Nature (Lond.).* 352:126–131.

Theriot, J. A., and T. J. Mitchison. 1992. Comparison of actin and cell surface dynamics in motile fibroblasts. *J. Cell Biol.* 118:367–377.

Yoneda, M. 1960. Force exerted by a single cilium of *Mytilus Edulis* I. *J. Exp. Biol.* 37:460–468.